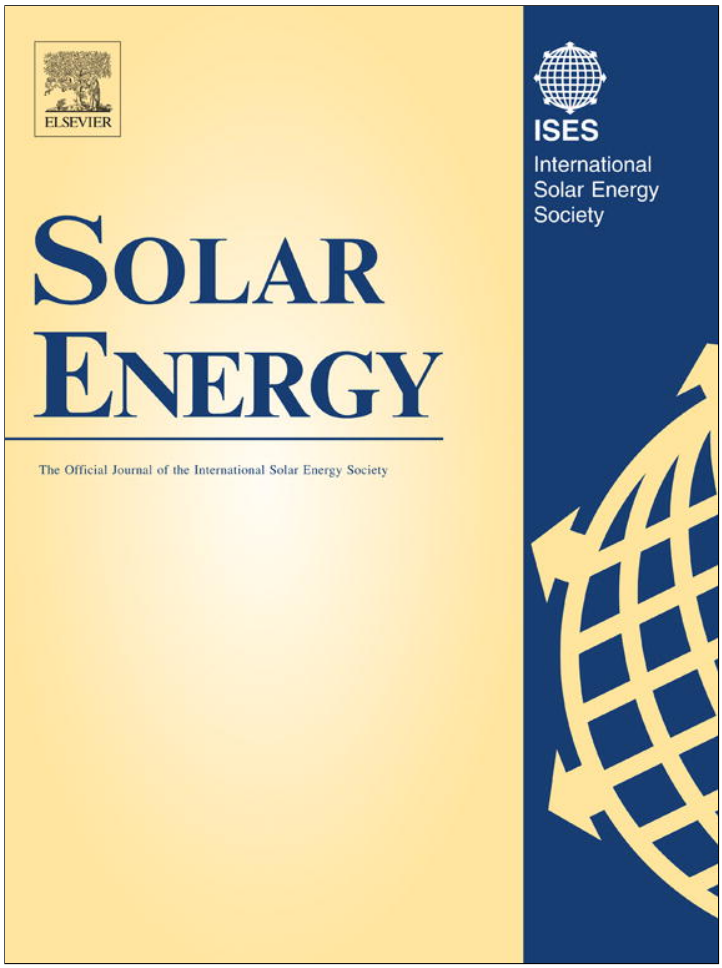

(This is a sample cover image for this issue. The actual cover is not yet available at this time.)

Available online at www.sciencedirect.com

SciVerse ScienceDirect

Solar Energy 88 (2013) 175–181

SOLAR ENERGY

www.elsevier.com/locate/solener

Comparison between textured SnO_2:F and Mo contacts with the p-type layer in p–i–n hydrogenate amorphous silicon solar cells by forward bias impedance analysis

G. Cannella [a], F. Principato [b,*], M. Foti [c], C. Gerardi [c], S. Lombardo [a]

[a] CNR-IMM, VIII strada, 5, 95121 Catania, Italy
[b] Dipartimento di Fisica, Università di Palermo, Edificio 18, Viale delle Scienze, 90128 Palermo, Italy
[c] ST-Microelectronics, Stradale Primosole, 50, 95121 Catania, Italy

Received 29 August 2012; received in revised form 25 November 2012; accepted 26 November 2012

Communicated by: Associate Editor Nicola Romeo

Abstract

In this paper we compare the performance of the textured SnO_2:F and Mo contacts with the p-type layer in p–i–n hydrogenate amorphous silicon (a-Si:H) solar cells. We use standard current–voltage (I–V) electrical characterization methods coupled with forward bias small signal impedance analysis. We show the efficacy of this technique to determine the effective carrier lifetime in photovoltaic cells. We show that such effective lifetimes are indeed directly connected to the respective dark diode saturation currents. We also find that the effective lifetime is constant with the temperature in the 0–70 °C range and it is significantly better for the solar cell with Mo diode contact. This also explains well the higher open circuit voltage V_{oc} found under illumination in the Mo/p–i–n cell compared to the SnO_2:F/p–i–n one.

Keywords: a-Si:H p–i–n solar cells; Impedance measurements; Effective carrier lifetime

1. Introduction

The importance of the contact between Transparent Conductive Oxide (TCO) and p-type a-Si:H has been intensively studied (Smole and Furlan, 1996; Dutta and Chatterjee, 2004; Dao et al., 2010) and it was demonstrated that at this interface the presence of a small barrier height at this interface, causes a decrease in the V_{oc} value and therefore in the solar cell performances (Dutta and Chatterjee, 2004). We have already studied the properties of the Mo and SnO_2:F interface with the p-type a-Si:H by studying the barrier height at the respective interface (Cannella et al., 2011a). We have demonstrated that the barrier height at the interface between Mo/p-type a-Si:H is 20 meV lower than that of SnO_2:F/p-type a-Si:H and that the V_{oc} of the Mo solar cell is 100 mV greater than that obtained with SnO_2:F as front contact (Foti et al., 2011). Moreover, in Lombardo et al. (2012) we have shown that the addition of an ultra-thin molybdenum film between the p-type a-Si:H film and the TCO/glass substrate in p–i–n a-Si:H solar cells causes an improvement of 10% in the internal quantum efficiency, due to the excitation of surface plasmon polariton modes at the a-Si:H/Mo interface.

In this work we perform an accurate electrical characterization under dark condition, by using current–voltage and forward bias small signal impedance, of the textured SnO_2:F and Mo contacts with the p-type layer in p–i–n a-Si:H solar cells. The small signal impedance under forward bias was used to determine the effective carrier lifetime τ_{eff} (Caverly and Ma, 1989; Schlangenotto and

* Corresponding author. Tel.: +39 091 23899027; fax: +39 091 23899063.
E-mail address: fabio.principato@unipa.it (F. Principato).

0038-092X/$ - see front matter © 2012 Elsevier Ltd. All rights reserved.
http://dx.doi.org/10.1016/j.solener.2012.11.019

Gerlach, 1969; Gatard et al., 2007; Caverly, 1998; Caverly and Hiller, 1990). Methodologies for the evaluation of the carrier lifetime in solar cells are important to characterize the carrier recombination mechanisms in photovoltaic devices. Different methods use the forward bias impedance of solar cells, even under illumination, to determine the carrier lifetime of the dominant recombination processes that occur in the device (e.g. Raniero et al., 2006). Although these methods allow to distinguish among different recombination mechanisms (e.g. bulk and interface states), they need detailed circuit models for assessing the mechanisms involved, especially in the case of the amorphous silicon, which has a complicated defects structure. In fact, the recombination is one of the main transport mechanisms in p–i–n a-Si:H solar cells (Deng and Wronski, 2005; Kind et al., 2011; van Berkel et al., 1993) and under dark forward bias it depends on the a-Si:H defects in mid-gap states just as in the case of photogenerated carrier recombination (Deng and Wronski, 2005). In p–i–n diode structures this recombination current depends on the injected carrier density in the intrinsic region and/or at the interface with the doped regions (Caverly and Ma, 1989; Schlangenotto and Gerlach, 1969). On the other hand, the DC forward bias current density (J) depends on the total injected charge density Q into the p–i–n diode through an effective carrier lifetime τ_{eff}, defined as $Q = J\tau_{eff}$. The τ_{eff} is the average time during which the electron–hole pair exists in the intrinsic layer (Caverly, 1998) and in the doped regions (Gatard et al., 2007).

In this work we determined the effective carrier lifetime in p–i–n a-Si:H photovoltaic cells with two different contacts with the p-type a-Si:H layer, Molybdenum (Mo) and textured SnO_2:F. We demonstrated that such measured effective lifetimes are indeed very well correlated to the relative DC dark recombination current values and to the performances of the photovoltaic cells under illumination.

2. Experimental procedures

The investigated SnO_2:F/p–i–n a-Si:H/ ZnO:Al (Aluminum doped Zinc Oxide, AZO) and Mo/p–i–n a-Si:H/ AZO structures were designed and realized by ST-Microelectronics (Catania, Italy). The two samples have different substrates: the former is the AGC ASAHI GLASS VU-type substrate with ≈700 nm thick SnO_2:F as TCO. The latter is composed by a an n-type Si wafer covered with SiO_2 for isolation on which a 700 nm nominal thickness Mo film is deposited by sputtering. The p–i–n a-Si:H cell were deposited on the two different substrates by plasma enhanced chemical vapor deposition (PECVD) at 255 °C. The top contact is a 1 μm nominal thickness AZO film deposited by sputtering. The final geometries were defined by photo-lithography and selective etching. The sheet resistances of SnO_2:F, AZO and Mo are, respectively, 5.0, 6.0 and 0.1 Ω/□. The cells are circular, with the following diameters: 0.01, 0.02, 0.04, 0.08, 0.16, 0.32, and 0.64 cm. In the rest of the paper, the Mo/p–i–n a-Si:H/AZO diode will be called Mo diode, while SnO_2:F/p–i–n a-Si:H/AZO will be called SnO_2:F diode.

The solar cells were first analyzed by measuring the J–V curves in dark condition with the two-points probe configuration in a probe station (Cascade), with the voltage varying in the −1 to 1 V range by using a HP 4156B semiconductor parameter analyzer. We studied also the J–V curves under illumination by using AM 1.5G solar simulator in the same voltage range and by using a Suss Microtech probe station. The impedance measurements were performed with an Agilent HP 4284A LCR meter, working in the 2T shielded configuration and with 30 mV rms A.C. signal. In particular, at fixed forward bias voltage, varying in the 0.4–0.85 V range, we selected the equivalent series resistance (R_s) and the reactance (X) of the LCR measurement parameters with the frequency varying in the range 10^2–10^6 Hz. From the values of R_s and X, for each bias voltage and frequency, we obtained the real and the imaginary part of the impedance, i.e. $Re(Z) = R_s$ and $Im(Z) = X$. We also measured the capacitance of the solar cells at 0.5 V reverse bias by configuring the LCR with the parallel conductance and capacitance measurement parameters.

All the measurements were performed in the 0–70 °C temperature range by using a thermostatic chuck with a Temptronic thermal controller working under N_2 flux.

3. The impedance model for the forward biased p–i–n diode

The small signal impedance method allows to evaluate the effective carrier lifetime in p–i–n device structures by the analysis of the impedance versus frequency measurements at different forward bias voltages. The p–i–n diode frequency dependent impedance Z is composed by three terms: $Z = Z_{PI} + Z_I + Z_{NI}$, where Z_{PI} and Z_{NI} are the junction impedances and Z_I is the impedance of the intrinsic layer of the p–i–n diode. To derive the expression of Z it is necessary to solve the ambipolar carrier transport equation with the boundary conditions at the PI and NI interfaces. The solution of the transport equation and expression of Z is given in Gatard et al. (2007). Z is a complex function of some diode physical and technological parameters, such as the ambipolar lifetime in the i-region (τ_I) and the width of the intrinsic region (W). At low frequencies ($\omega\tau_I \ll 1$) Z is essentially resistive and is given by

$$Z \approx R_{LF} = \eta V_T / J, \tag{1}$$

where V_T is the thermal voltage and η is the ideality factor of the diode. On the contrary, at high frequency ($\omega\tau_I \gg 1$), the injected carrier density is concentrated close to the doped regions and the i-layer contribution to Z dominates. It mainly depends on the W/L ratio, where L is the ambipolar diffusion length. In particular, when $W/L > 2$ then the imaginary part of impedance is inductive, while if $W/L < 2$ then it is capacitive because the diffusion capacitance dominates. In the latter case the reactance versus

frequency shows a minimum (f_{min}) (Caverly and Ma, 1989; Gatard et al., 2007; Varshney et al., 1974). The inverse of f_{min} is the effective carrier lifetime τ_{eff}, hence

$$\tau_{eff} = 1/2\pi f_{min}. \quad (2)$$

Assuming that the lifetimes in the two doped regions are equal and denoting them with τ_E, the effective p–i–n diode lifetime may be written as Schlangenotto and Gerlach (1969):

$$\frac{1}{\tau_{eff}} = \frac{1}{\tau_I} + \frac{Q_E}{Q_I \tau_E}, \quad (3)$$

where $Q_{E(I)}$ is the charge stored in the doped (intrinsic) region. In particular at high carrier injection levels, the effective lifetime is (Caverly and Ma, 1989):

$$\frac{1}{\tau_{eff}} = \frac{1}{\tau_I} + \frac{2hJ\tau_I}{qW^2}, \quad (4)$$

where $h = \sqrt{D_E \tau_E}/N_E$ is a parameter that takes into account recombination in the doped regions (Caverly and Ma, 1989; Schlangenotto and Gerlach, 1969; Gatard et al., 2007), D_E and N_E are the diffusion coefficient and the doping in the doped regions, respectively.

4. Results and discussion

Fig. 1 shows the scanning electron micrograph (SEM) images of the SnO_2:F (a) and Mo (b) diode. The Mo diode shows an almost planar structure, while the layers of the SnO_2:F diode are not flat, because each of the layers deposits conformally over the textured SnO_2:F layer. The cross section images of both devices approximately confirm the nominal thickness of the AZO and Mo layer and show that the overall p–i–n a-Si:H thickness is about 300 nm. To better investigate the surface morphology of the SnO_2:F layer atomic force microscopy (AFM) was used. Fig. 2 shows the AFM image taken on a SnO_2:F/glass sample. The rms roughness is 29 nm, which is a typical value for SnO_2 ASAHI layers used in thin film silicon solar cells (Zeman et al., 2000).

Fig. 3 shows the measured capacitance normalized with respect to the nominal area $\pi d^2/4$, where d is the nominal circular pad diameter, as a function of frequency at reverse bias of 0.5 V and at room temperature. We note that at low frequency the SnO_2:F diode has a higher capacitance compared to that of the Mo diode, with a ratio of the low frequency capacitances $C_{SnO_2}/C_{Mo} \cong 1.1$. This difference may be due to a larger effective area in the SnO_2:F diode caused by the textured surface of the SnO_2:F as shown in Fig. 2.

In the SnO_2:F diode the reverse capacitance decreases at frequencies higher than 500 kHz and for device diameters greater than 800 μm. Indeed, the impedance (admittance) of the solar cells is measured with metal probes, which contact the TCO. The TCO resistivity can cause a voltage drop along the TCO layer. In our case the SnO_2:F TCO resistivity is one order of magnitude higher than that of the Molybdenum and causes the capacitance drop at high frequencies and for large area pads (Principato et al., 2010; Cannella et al., 2011b). To avoid the effects of the TCO sheet resistance on the impedance measurements we have studied only devices with diameters less than 800 μm and at frequencies lower than 500 kHz.

Fig. 4 shows the real part of the impedance versus frequency at different voltages for the Mo diode (a) and for the SnO_2:F diode (b). In both devices for voltages higher than 0.65 V and 0.55 V for the Mo and the SnO_2:F diode, respectively, we can estimate the low frequency resistance R_{LF} because $Re(Z)$ shows a plateau. The measured value

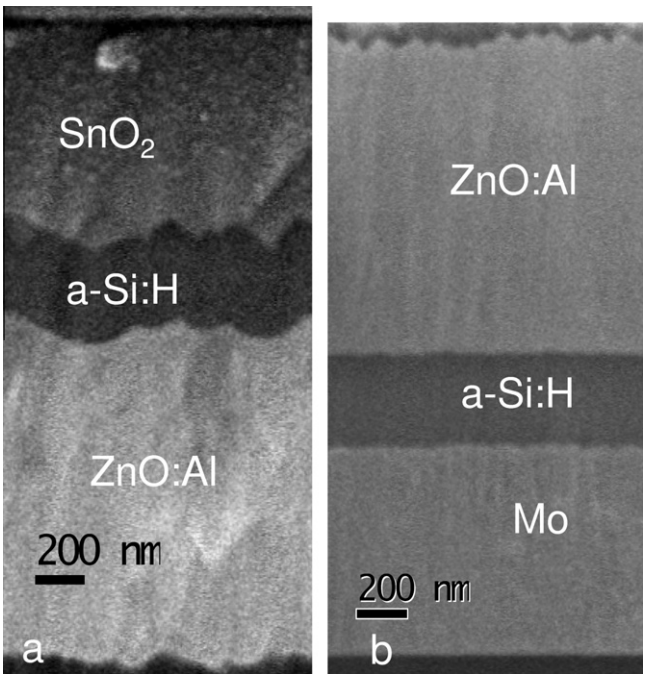

Fig. 1. SEM images of the SnO_2:F (a) and Mo (b) diode.

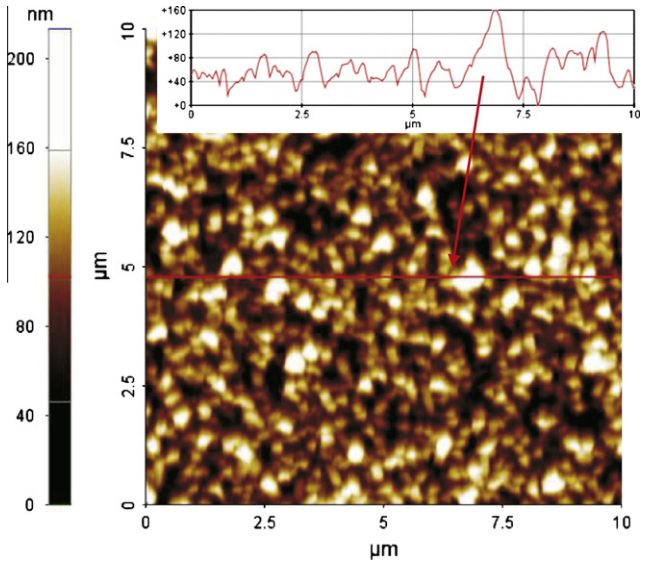

Fig. 2. AFM picture taken on a SnO_2:F/glass sample. The rms roughness is about 29 nm.

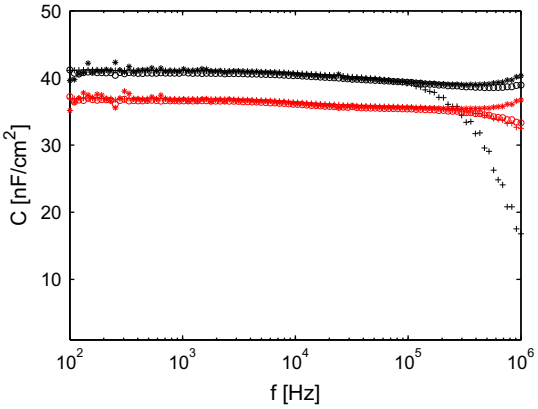

Fig. 3. Capacitance versus frequency measured at a reverse bias of 0.5 V for Mo (red) and SnO_2:F (black) diode for different cell diameters: 200 μm (*), 400 μm (○) and 800 μm (+). (For interpretation of the references to color in this figure legend, the reader is referred to the web version of this article.)

of $Re(Z)$ at 100 Hz is very close to that estimated from Eq. (1) by using the ideality factor determined from D.C. current–voltage measurements. However, both for the Mo and the SnO_2:F diode, we are not able to evaluate the high frequency resistance of the p–i–n diode since in the former $Re(Z)$ does not show any plateau, while in the latter the plateau at about 0.8 Ω cm^2 is due to the SnO_2:F sheet resistance, because this value increases with the device diameter (not shown).

Fig. 5 shows $-Im(Z)$, i.e. the imaginary part of the impedance changed of sign to be positive, measured at room temperature as a function of frequency at different voltages for the Mo (a) and the SnO_2:F diode (b). At the lowest voltages $-Im(Z)$ does not have any maximum in the 10^2–10^6 Hz frequency range, but when the bias voltage increases, the maximum of $Im(Z)$ is clearly observed and the f_{min} value increases for both diodes. At high frequency, for both the types of diode, $-Im(Z)$ decreases with frequency and it tends to collapse in a single curve for all voltages. Fig. 6 shows the inverse of the effective carrier lifetime obtained by using Eq. (4) as a function of the current density for both the Mo and SnO_2:F diodes. We noticed that the effective lifetime in the Mo diode is higher than that found in the SnO_2:F diode. By using Eq. (4) we performed a linear fit of the data to the relationship: $1/\tau = A + B\,J$, where A and B are fitting parameters (black lines in Fig. 6). We found for the Mo diode $B = 2.35 \pm 0.2 \times 10^8$ s cm^2/A and $A = 470$ s^{-1} and for the SnO_2:F, $B = 4.33 \pm 0.4 \times 10^8$ s cm^2/A and $A = 244$ s^{-1}. The absence of a

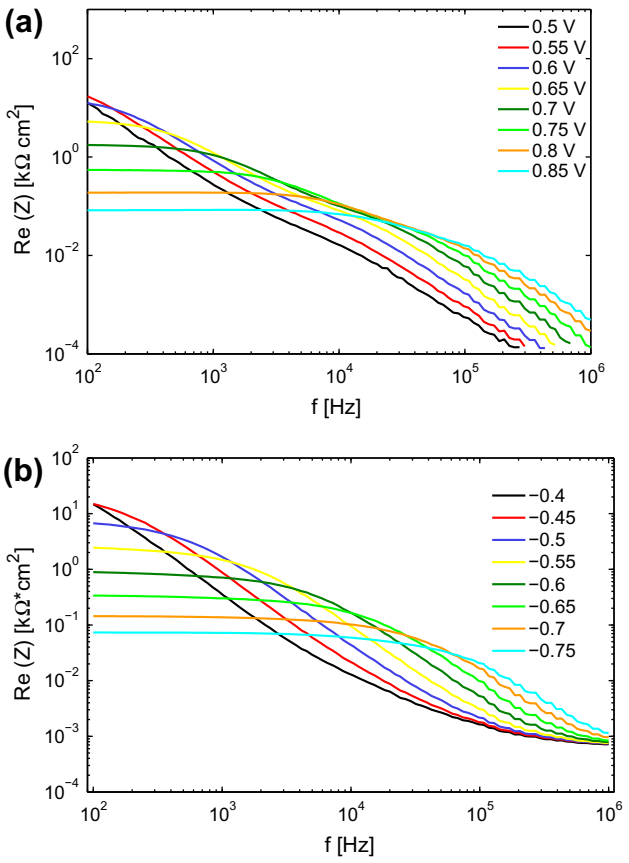

Fig. 4. Real part of the impedance as a function of the frequency measured at different forward bias voltages for (a) Mo and (b) SnO_2:F diode.

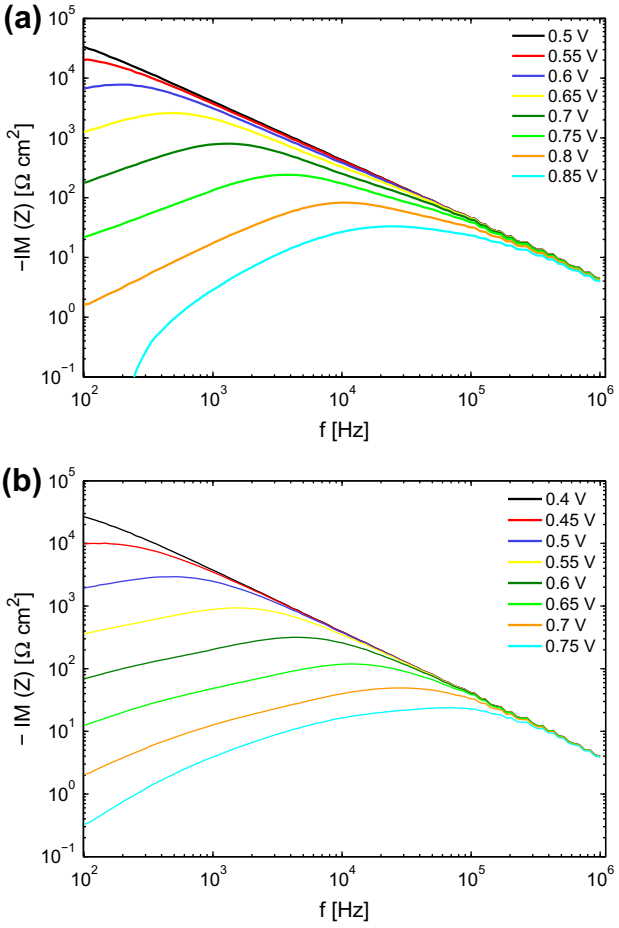

Fig. 5. Imaginary part of the impedance, changed of sign, as a function of the frequency measured at different forward bias voltages for (a) Mo and (b) SnO_2:F diode.

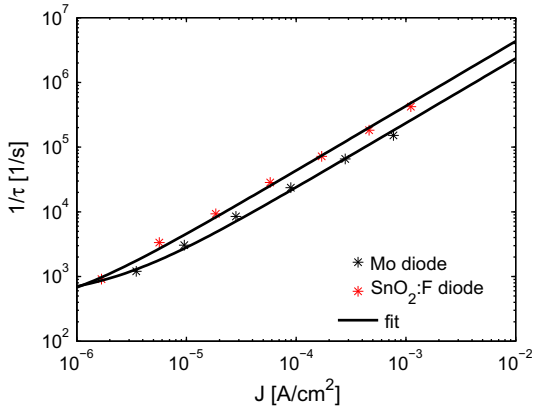

Fig. 6. Inverse of the effective lifetime measured at different values of J for Mo (black star) and SnO_2:F (red star) diodes at room temperature. The continuous lines are obtained with the fitting of Eq. (4). (For interpretation of the references to color in this figure legend, the reader is referred to the web version of this article.)

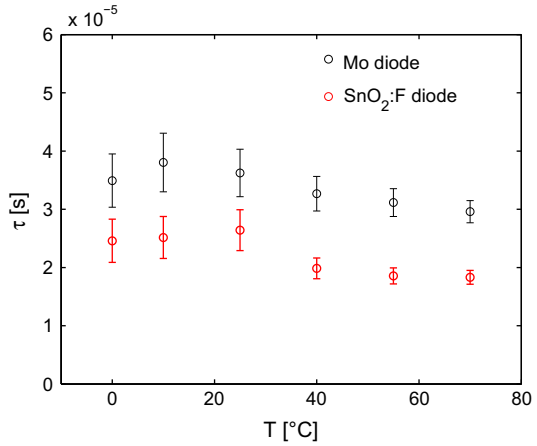

Fig. 7. Effective lifetime at a forward current density of 80 μA/cm^2 for Mo (black) and SnO_2:F (red) diodes at different temperatures. (For interpretation of the references to color in this figure legend, the reader is referred to the web version of this article.)

plateau at low current density causes a high error in the determination of the parameter A, thus the τ_I cannot be determined. Hence, the ratio of the effective lifetimes at same bias current of the Mo and SnO_2:F diodes is approximately given by the ratio between the two values of B found from the previous fitting:

$$\frac{\tau_{eff,\mathrm{Mo}}}{\tau_{eff,\mathrm{SnO_2}}} \cong \frac{B_{\mathrm{SnO_2}}}{B_{\mathrm{Mo}}} = 1.84.$$

We have also studied the effective lifetime at different temperatures and at fixed current. Fig. 7 shows the lifetimes obtained in the 0–70 °C temperature range for the Mo (black) and the SnO_2:F diode (red) at a forward bias current density of 80 μA/cm^2. The measured lifetime values are 33.8 ± 3.2 and 22.1 ± 3.6 μs for Mo and SnO_2:F diodes respectively, and are both almost constant with the temperature. The lack of a clear temperature dependence of the

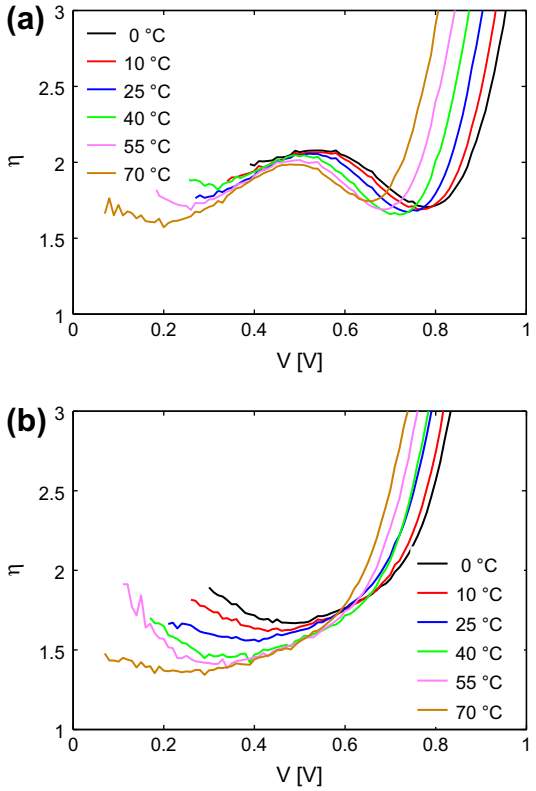

Fig. 8. Ideality factor $\eta(V)$ at different temperatures for (a) Mo and (b) SnO_2:F of 400 μm diameter solar cells.

effective lifetimes is likely due to the limited investigated temperature range, hence the lifetime variations are probably hidden within the experimental uncertainty. The reproducibility of these results was also demonstrated not only on solar cells made on the same wafer but also on different wafers to test the goodness and the uniformity of the used deposition processes. By considering Eq. (4) such a difference may be due either to a different intrinsic region lifetime parameter τ_I or to a different recombination parameter h related to the different structure of the p^+ regions, planar in the Mo diode and textured in the SnO_2:F device.

To better understand the difference of two types of solar cells we analyzed the diode ideality factors. Fig. 8 shows the values of the ideality factor as a function of the bias voltage and at different temperatures of the Mo (a) and SnO_2:F (b) diodes. In general, the ideality factor as a function of the bias shows some artifacts at low and high voltages due to the effects of the leakage and series resistance, respectively. We note that, in voltage range where these artifacts are negligible, compared to the Mo diode, the SnO_2:F device shows lower values of the ideality factor reaching values down to about 1.5. Indeed, the ideality factor in such devices has a strong relationship with the charge transport mechanisms. If the carrier recombination in the p–i–n is dominated by the p/i or n/i interface the current is ruled by the interface recombination velocity and the current in this case has an exponential shape with the

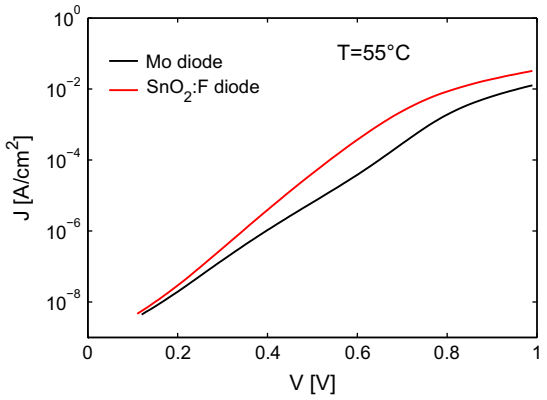

Fig. 9. Current–voltage curves for Mo (black) and SnO_2:F (red) diodes at $T = 55$ °C. (For interpretation of the references to color in this figure legend, the reader is referred to the web version of this article.)

$\eta \approx 1$ and almost independent of bias (van Berkel et al., 1993). On the contrary, when the transport mechanism is dominated by recombination through a single defect level in the i-layer, the ideality factor $\eta \approx 2$ as predicted by SRH theory (Sze, 1981). Hence, the lower value of the ideality factor of the SnO_2:F diode, suggests that the recombination at the interface is more relevant in this structure with respect to the Mo diode. In other words the recombination rate at the p/i interface is lower in the Mo diode. Such conclusion is confirmed by the results of the impedance analysis. In fact, if we assume that the carrier lifetimes τ_I and the mobility in the doped region are similar for both diodes and by taking into account for the expression of the parameter h, the ratio between the effective lifetimes of two investigated structures can be expressed as (from Eq. (4))

$$\frac{\tau_{eff,\mathrm{Mo}}}{\tau_{eff,\mathrm{SnO_2}}} \cong \frac{(h\tau_I)_{eff,\mathrm{SnO_2}}}{(h\tau_I)_{eff,\mathrm{Mo}}} \cong \sqrt{\frac{\tau_{E,\mathrm{Mo}}}{\tau_{E,\mathrm{SnO_2}}}} \cong 1.84.$$

Hence, the minority carrier lifetime in the doped region of the SnO_2:F diode is lower than that of Mo diode. The better quality of the Mo/p-aSi:H contact respect to that of the SnO_2:F/p-aSi:H is also confirmed by the dark J–V curves for both diodes as shown in Fig. 9. The current at the same voltage is lower in the Mo diode, indicating a lower carrier recombination rate. The better quality of the TCO/p-type and p/i interfaces of the Mo diode is also confirmed by the values of V_{oc} and short circuit current densities J_{sc} measured under standard illumination conditions. In fact, we measured 0.88 V and 6.0 mA/cm^2 for the Mo diode and 0.78 V and 9.0 mA/cm^2 for the SnO_2:F (Foti et al., 2011). In order to better understand the J_{sc} difference we estimate the value of the series resistance from the measured J–V curves in dark. The values of the series resistances are very similar and $\approx 12\ \Omega\ \mathrm{cm}^2$ for both diodes. Generally, the series resistance of p–i–n solar cells is the sum of two contributions: one due to the resistivity of the p and n layers and the other due to the sheet resistance of the TCO and/or Mo layers. The latter predominate for large area cells, of diameter above 1600 μm (Principato et al., 2010). Hence, the series resistance, in our case, for sizes equal or below 800 μm, is mainly due to the p-type and n-type a-Si:H layers for both Mo and SnO_2:F diodes. Hence, the J_{sc} difference between the two type of diodes cannot be explained by series resistance differences. Thus, we attribute the large J_{sc} variation to the textured surface of the SnO_2:F layer, which produces some light trapping effect (Zeman et al., 2000).

The higher V_{oc} in the Mo diode can be explained by considering the well known expression of the open circuit voltage

$$V_{oc} = \eta \ln\left(\frac{J_{sc} - J_{rec}}{J_0}\right), \tag{5}$$

where J_0 is the saturation current density and J_{rec} is the recombination current (Merten et al., 1998). Thus, although the solar cell with the SnO_2:F contact has a higher value of J_{sc} than that of the Mo contact, the higher value of the SnO_2:F interface recombination rate increases both J_{rec} and J_0, thus reducing V_{oc}. We conclude that the V_{oc} difference between the two types of cells is mainly caused by the minority carrier lifetime difference in the p-type a-Si:H due to the contacts with Mo or SnO_2:F. We have already demonstrated that there is a barrier height difference of 20 mV between Mo and SnO_2:F/p interface (Cannella et al., 2011a). This different barrier height contributes to the lower V_{oc} in SnO_2:F diode, but it is reasonable to think that the two devices differ mainly for the p/i interface of the a-Si:H film since the PECVD conditions are identical in the two cases, only the substrates are different, and the PECVD of the a-Si:H starts with the deposition of the 20 nm thick p-type layer. This process is more aggressive in the case of the SnO_2:F compared to the Mo substrate, since the Mo is a refractory metal.

5. Conclusion

We have studied the influence of the Mo and SnO_2:F contacts with p-type a-Si:H in a-Si:H p–i–n solar cells. We have performed $Z - f$ measurements in dark condition and at different temperatures (0–70 °C) and forward bias voltages to study the effective lifetime in these diodes by applying a model originally developed for RF and microwave p–i–n diodes (Caverly and Ma, 1989; Schlangenotto and Gerlach, 1969; Gatard et al., 2007; Caverly, 1998; Caverly and Hiller, 1990). In this work we applied this small signal impedance method to p–i–n a-Si:H solar cells with two different contacts with the p-type a-Si:H layer. The effective lifetimes as a function of the forward bias current density actually follow quite well the linear dependence predicted by the model of Eq. (4). We found that in the investigated current range the Mo diode has a higher effective carrier lifetime. This is consistent with the lower saturation current J_0 observed from the dark J–V characteristics and the higher V_{oc} measured under standard illumination conditions in the Mo diode compared to the SnO_2:F diode.

We conclude that the method of analysis of the Z versus frequency data applied to the case of a-Si:H solar cells is an useful, effective, and simple tool to evaluate the effective carrier lifetime and the overall quality of the p–i–n materials for solar cells.

Acknowledgments

This work has been carried out with partial funding support of STMicroelectronics. We gratefully acknowledge the team of the IMS R&D of ST-Microelectronics (S. Coffa, S. Ravesi, C. Tringali, N. Sparta, S. Di Marco, and A. Grasso) for help in the research development and S. Scalese, M. Italia and P. Fiorenza of the IMM-CNR for the SEM and AFM images.

References

Cannella, G., Principato, F., Foti, M., Marco, S.D., Grasso, A., Lombardo, S., 2011a. Journal of Applied Physics 110, 024502, p. 8.
Cannella, G., Principato, F., Foti, M., Garozzo, C., Lombardo, S., 2011b. Energy Procedia 3, 51.
Caverly, R., 1998. Electronics Letters 34, 2277.
Caverly, R.H., Hiller, G., 1990. Solid-State Electronics 33, 1255.
Caverly, R.H., Ma, X., 1989. Solid-State Electronics 32, 329.
Dao, V.A., Heo, J., Choi, H., Kim, Y., Park, S., Jung, S., Lakshminarayan, N., Yi, J., 2010. Solar Energy 84, 777.
Deng, J., Wronski, C.R., 2005. Journal of Applied Physics 98, 024509.
Dutta, U., Chatterjee, P., 2004. Journal of Applied Physics 96, 2261.
M. Foti, G. Cannella, C. Gerardi, S. Di Marco, S. Ravesi, N. Sparta, S. Lo Verso, F. Principato, S. Coffa, and S. Lombardo, in: Proc. ECS Trans., vol. 41, 2011, pp. 15–20.
Gatard, E., Sommet, R., Bouysse, P., Quere, R., 2007. IEEE Microwave and Wireless Components Letters 17, 211.
Kind, R., van Swaaij, R.A.C.M.M., Rubinelli, F.A., Solntsev, S., Zeman, M., 2011. Journal of Applied Physics 110, 104512.
Lombardo, S., Tringali, C., Cannella, G., Battaglia, A., Foti, M., Costa, N., Principato, F., Gerardi, C., 2012. Applied Physics Letters 101, 123902, p. 4.
Merten, J., Asensi, J., Voz, C., Shah, A., Platz, R., Andreu, J., 1998. IEEE Transactions on Electron Devices 45, 423.
Principato, F., Cannella, G., Lombardo, S., Foti, M., 2010. Solid-State Electronics 54, 1284.
Raniero, L., Fortunato, E., Ferreira, I., Martins, R., 2006. Journal of Non-Crystalline Solids 352, 1880.
Schlangenotto, H., Gerlach, W., 1969. Solid-State Electronics 12, 267.
Smole, M.T.F., Furlan, J., 1996. Journal of Non-Crystalline Solids 194, 312.
Sze, S.M., 1981. Physics of Semiconductor Devices, second ed. J. Wiley & Sons.
van Berkel, C., Powell, M.J., Franklin, A.R., French, I.D., 1993. Journal of Applied Physics 73, 5264.
Varshney, R., Roulston, D., Chamberlain, S., 1974. Solid-State Electronics 17, 699.
Zeman, M., van Swaaij, R.A.C.M.M., Metselaar, J.W., Schropp, R.E.I., 2000. Journal of Applied Physics 88, 6436.